RSC Advances

PAPER

View Article Online
View Journal | View Issue

Cite this: *RSC Adv.*, 2020, **10**, 34806

Novel TiO_2/GO/$CuFe_2O_4$ nanocomposite: a magnetic, reusable and visible-light-driven photocatalyst for efficient photocatalytic removal of chlorinated pesticides from wastewater†

A. M. Ismael,‡[a] A. N. El-Shazly, ‡*[b] S. E. Gaber,[a] M. M. Rashad,[b] A. H. Kamel[c] and S. S. M. Hassan[c]

A TiO_2/GO/$CuFe_2O_4$ heterostructure photocatalyst is fabricated by a simple and low-cost ball-milling pathway for enhancing the photocatalytic degradation of chlorinated pesticides under UV light irradiation. Based on the advantages of graphene oxide, TiO_2, and $CuFe_2O_4$, the nanocomposite exhibited visible light absorption, magnetic properties, and adsorption capacity. Integrated analyses using XRD, SEM, TEM, and UV-visible techniques demonstrated that the nanocomposite exhibited a well-defined crystalline phase, sizes of 10–15 nm, and evincing a visible light absorption feature with an optical bandgap energy of 2.4 eV. The photocatalytic degradations of 17 different chlorinated pesticides (persistent organic pollutants) were assayed using the prepared photocatalyst. The photocatalytic activity of the nanocomposite generated almost 96.5% photocatalytic removal efficiency of typical pesticide DDE from water under UV irradiation. The superior photocatalytic performance was exhibited by the TiO_2/GO/$CuFeO_4$ catalyst owing to its high adsorption performance and separation efficiency of photo-generated carriers. The photocatalyst was examined in 5 cycles for treating uncolored pesticides with purposeful separation using an external magnetic field.

Received 29th March 2020
Accepted 6th August 2020

DOI: 10.1039/d0ra02874f

rsc.li/rsc-advances

1. Introduction

Water pollution has become one of the most dangerous issues that threaten our world because of its severe impact on human health and the whole ecosystem.[1,2] There are various major classes of water pollutants such as heavy metal ions, textile dyes, phenols, fertilizers, and pesticides that are responsible for contamination of both groundwater and surface water.[3,4] Due to their high toxicity, long durability, and resistance to degradation by traditional methods, pesticides could be considered as one of the most common organic pollutants.[5,6] Advanced oxidation processes are the most effective strategies proposed for wastewater treatment because of their ability to completely degrade persistent organic pollutants.[7,8] Semiconductor-based photocatalysis has been known as a green, simple, and cost-effective technique for the complete degradation of organic contaminants, as well as being efficiently utilized in various other photocatalytic applications, hydrogen production, carbon dioxide reduction and solar cell water splitting.[9–12]

Titanium dioxide (TiO_2) is a much used photocatalyst because it is non-toxic, chemically and photochemically stable, readily available, and easy to synthesize.[13,14] However, TiO_2 has two major demerits: it possesses a wide bandgap energy value of 3.2 eV for pure anatase, which limits its activity under UV irradiation, and it exhibits rapid electron–hole recombination, which decreases its photocatalytic performance.[15,16] Various strategies, including doping by metallic/nonmetallic species, dye sensitization, as well as coupling with narrow bandgap semiconductors, have been developed to expand its photoresponse into the visible light region, decrease electron–hole pair recombination and increase its activity for the removal of toxic pollutants from industrial effluents.[17–19]

Besides, an improvement in the photocatalytic activity of TiO_2 has been obtained by loading with carbonaceous materials, especially graphene and graphene oxide (GO), as promising supports for photocatalysts owing to their high carrier mobility and large specific surface area, allowing them consideration.[20–23] It is noted that in previous studies on graphene/TiO_2 and GO/TiO_2 nanocomposites, they displayed an excellent performance in the destruction of organic dyes using both ultraviolet and visible light radiation when compared to pure

[a]National Water Research Center, P. O. Box 74, 13411, Shoubra El-Kheima, Egypt. E-mail: ayatelshazly@gmail.com; saadsmhassan@yahoo.com; rashad133@yahoo.com

[b]Central Metallurgical Research and Development Institute (CMRDI), P. O. Box 87, Helwan, 11422, Cairo, Egypt

[c]Department of Chemistry, Faculty of Science, Ain Shams University, Cairo, Egypt

† Electronic supplementary information (ESI) available. See DOI: 10.1039/d0ra02874f

‡ These authors contributed equally to this work.

TiO_2 due to the synergetic effects caused by graphene.[24,25] Graphene is generally used as an efficient electron acceptor for photo-induced charge carriers, thus significantly suppressing the recombination of photo-generated electron–hole pairs and enhancing the performance of the nanocomposite.[26]

To facilitate the separation of photocatalyst material for recycling, a TiO_2 photocatalyst could be modified by coupling with magnetic material, which can be facilely isolated from solution by inducing an external applied magnetic field.[27,28] It was reported that the incorporation of Fe_3O_4 and spinel ferrites such as $CoFe_2O_4$, $NiFe_2O_4$, or $ZnFe_2O_4$ into TiO_2 could cause a change in its magnetic properties and allow the easy recovery of photocatalysts.[28–31] Although spinel-structured materials exhibit photocatalytic properties, they have low valence band offsets and poor photoelectric performance. That is attributed to the insufficient energy for the reduction of molecular oxygen by photo-induced electrons, which is the primary electron scavenger in most photocatalytic reaction systems. Therefore, the improvement in the performance of TiO_2 using spinel ferrites could not be accredited to the photocatalytic activity of the spinel ferrites, but it results from the extension of the visible light response of the combined system with charge transfer behavior.[32]

From the environmental point of view, enhancing the photoresponse and improving the visible light absorption spectrum, the coupling between semiconductor nanocomposites and graphene looks tremendously meaningful. Thus, it is supposed that the fabrication of a heterostructure photocatalyst of TiO_2, $CuFe_2O_4$, and GO is promising; the combination of $CuFe_2O_4$ and TiO_2 with p–n heterojunction can enhance the absorption of TiO_2 to the visible light region. Also, supporting both of them with a GO matrix would increase the absorptivity of the pollutants and enhance the charge separation efficiency of TiO_2 and allow easy separation from solution. Thus, herein, we demonstrate a simple one-pot method to synthesize a ternary nanocomposite based on TiO_2/GO/$CuFe_2O_4$ to be used as an effective photocatalyst to remove pesticides from wastewater. The proposed nanocomposite possesses multiple functions where TiO_2 represents the main active phase, GO provides an electron transition pathway to reduce recombination rate in TiO_2 and enhance its photocatalytic activity, while $CuFe_2O_4$ as a magnetic material allows separation of the prepared nanocomposite. To the best of our knowledge, this is the first report of the effect of TiO_2/GO/$CuFe_2O_4$ nanocomposite as a smart photocatalyst toward photodegradation of 17 types of pesticide. The as-prepared nanocomposite was characterized using XRD, SEM, TEM, and DRS. We confirmed the photocatalytic response of the as-prepared photocatalyst under UV light as well as easy separation and high performance, where it showed promising results for the removal of pesticides from wastewater.

2. Experimental

2.1. Materials

Spinel-structured copper ferrite ($CuFe_2O_4$) powders have been synthesized using the co-precipitation method. Chemical grade iron(III) nitrate nonahydrate, $Fe(NO_3)_3 \cdot 9H_2O$, and copper(II) nitrate, $Cu(NO_3)_2 \cdot 6H_2O$, were used as the starting materials. Sodium hydroxide (NaOH, ADWIC 98%) and hydrochloric acid (HCl, ADWIC 33%) were utilized for pH adjustment. Graphite powder (Alfa Aesar), sulfuric acid (H_2SO_4, 99.9%, Sigma-Aldrich), potassium permanganate ($KMnO_4$, Analar analytical grade), and potassium nitrate (KNO_3, ACROS) were used for the preparation of graphene. Titanium isopropoxide [$Ti(OCH(CH_3)_2)_4$] (99.99%) was used to synthesize anatase TiO_2 nanoparticles using the hydrothermal route. Standard reference chlorinated pesticides (AccuStandard, USA), *n*-hexane (HPLC-isocratic grade, Sigma-Aldrich), dichloromethane (HPLC grade, Sigma-Aldrich) and anhydrous sodium sulfate (ACS Reagent Grade, MP Biomedicals, LLC, France) were used.

2.2. Synthesis of the heterostructure photocatalyst

2.2.1. Synthesis of $CuFe_2O_4$. Copper ferrite nanoparticles were synthesized by the co-precipitation method using $Cu(NO_3)_2 \cdot 6H_2O$ (0.01 mol) and $Fe(NO_3)_3 \cdot 9H_2O$ (0.02 mol) in stoichiometric amounts as starting materials. Then, the precipitation was performed by slowly adding NaOH (1 M) until pH was equal to 8. After complete precipitation, the resulting product was washed several times by distilled water and dried at 60 °C overnight. The sample was annealed at 800 °C for 2 h.

2.2.2. Synthesis of GO. GO was produced using the modified Hummers method from pure graphite powder. Typically, 27 mL of sulfuric acid (H_2SO_4) and 3 mL of phosphoric acid (H_3PO_4) (volume ratio 9 : 1) were mixed to get a homogenous solution. Then 0.225 g of graphite powder was added into the mixed solution under stirring condition. 1.32 g of potassium permanganate ($KMnO_4$) was then added slowly into the solution. This mixture was magnetically stirred for 6 h until the solution became dark green. After that, 2 g of KNO_3 was added to the solution after 15 min. This solution was then stirred at room temperature for 2 h. Later 200 mL of distilled water was added to the solution. 10 mL of 30% H_2O_2 was dropped slowly, and 600 mL of distilled water was added to the solution. The filtrate obtained was washed with HCl (10%). The brown suspension obtained was heated in a muffle furnace for 30 min at 60 °C and then allowed to cool overnight in air.

2.2.3. Synthesis of TiO_2. The TiO_2 nanoparticles were prepared *via* a hydrothermal method. 25 mL titanium isopropoxide [$Ti(OCH(CH_3)_2)_4$] was added to 100 mL of distilled water under vigorous stirring for 10 min with ammonium hydroxide at pH 7. After stirring for another 10 min, the mixed solution was transferred to a 150 mL Teflon-lined stainless steel autoclave. The autoclave was kept in an electric oven at 100 °C for 24 h. After cooling down to room temperature, samples were washed with deionized water several times and dried at 80 °C for 10 min.

2.2.4. Synthesis of the TiO_2/GO/$CuFe_2O_4$ nanocomposite. Initially, 5 g of TiO_2 powder was blended with 2.5 g GO and 2.5 g $CuFe_2O_4$ powder to produce the TiO_2/GO/$CuFe_2O_4$ nanocomposite. Then, a 10 g portion of the mixture was thoroughly mixed with 20 g zirconia in a grinding bowl. The weight ratio of the product material per ball was 1 : 10. The ball-milling process was carried out at 550 rpm for 3 h.

2.3. Physical characterization

Powder X-ray diffraction (XRD) was carried out using a Bruker AXS diffractometer (D8-ADVANCE, Germany) with Cu Kα (λ = 1.54056 Å) radiation, operating at 40 kV and 40 mA. The diffraction data were recorded for 2θ values between 10 and 80°. The morphologies of the prepared samples were directly observed *via* field emission scanning electron microscopy (SEM) with a JSM-7800F instrument (JEOL, Japan). Transmission electron microscopy (TEM) images were obtained using a 2010F instrument (JEOL, Japan). The UV-visible-NIR absorption spectra were recorded using a spectrophotometer with diffuse reflectance configuration. The measurements were performed using a V-570 spectrophotometer (Jasco, Japan), with an integrating sphere reflectance unit.

2.4. Photocatalytic degradation of pesticides

The prepared photocatalyst was transferred to a quartz reaction cell containing an aqueous solution of the test chlorinated pesticides. A 150 W xenon arc lamp with wavelength of 365 nm (CHF-XQ-500W, Beijing Changtuo Co. Ltd) was immersed in the cell and used as a UV radiation source. After 20 min of immersion and pesticide adsorption on the catalyst, the photocatalytic degradation of the pesticides was followed using a GC-MS system (Agilent 7890A) coupled with a 5975C triple-quadrupole MS and a computer with MassHunter software (version B.05.00412) for data acquisition and processing (Agilent Technologies). The GC system was equipped with a 7693 autosampler and an air-cooled multimode inlet. The injection volume was 1.0 μL in splitless mode. Analytes were separated with two HP-5 ms Ultra Inert capillary columns from Agilent (30 m × 250 μm × 0.25 μm), connected at a backflush union. The column head pressure was set at 9.3825 psi at a constant flow rate of 1.0 mL min^{-1}, using helium as a carrier gas. The column temperature was programmed as follows: the initial temperature was 80 °C (for 1.0 min hold time) and increased to 175 °C at 30 °C min^{-1} (for 4.0 min hold time), ramped to 225 °C at 3 °C min^{-1} (for 6.0 hold time). The total run time was 30.9 min. By GC-MS, we can analyze the pesticides before UV irradiation and after UV irradiation. Removal of pesticide from water is evaluated by using 6630B method (liquid–liquid extraction gas-chromatography) then take 1 mL to analyze it. Table 1 presents the results after UV irradiation at various times and different concentrations of 0.1, 0.15, and 0.05. Thus, the concentration of the decomposed pesticides was measured as a function of irradiation time and compared with a calibration graph previously constructed.

3. Results and discussion

3.1. Characterization of TiO_2/GO/$CuFe_2O_4$ nanocomposite

The crystal structure of the prepared TiO_2/GO/$CuFe_2O_4$ nanocomposite was investigated using XRD analysis. The XRD profile of TiO_2/GO/$CuFe_2O_4$ nanocomposite reveals the presence of crystalline anatase TiO_2 peaks with no extra detectable peaks in the diffraction pattern for GO and $CuFe_2O_4$ (Fig. 1a). This indicated the presence of relatively low percentage of GO and $CuFe_2O_4$ in the nanocomposite. On the other hand, the EDX spectrum of the composite (Fig. 1b) demonstrates the presence of Ti, Cu, C, Fe, and O elements, distinctly elucidating that GO and $CuFe_2O_4$ existed in the nanocomposite.

SEM and TEM analyses were used to analyze the morphology of the nanocomposite. The SEM image (Fig. 2a) shows that TiO_2/GO/$CuFe_2O_4$ particles were of inhomogeneous size and aggregated together. Fig. 2b–d display the TEM images at different magnifications in which a clear uniform dispersion of TiO_2 and $CuFe_2O_4$ nanoparticles with a size of ~15 nm (Fig. 2b) on the GO nanosheets was formed in the process of ball milling. Also demonstrated was a prospective electrostatic attraction between GO, TiO_2, and $CuFe_2O_4$ nanoparticles. Meanwhile, TiO_2 and $CuFe_2O_4$ covered the surface of the GO nanosheets, as also presented in Fig. 2c and d.

The TiO_2/GO/$CuFe_2O_4$ nanocomposite was further characterized using UV-visible diffuse reflectance spectroscopy, and the results are depicted in Fig. 3a. TiO_2 displayed a light response over the range of 300–400 nm, which is probably due to the band-to-band transition of anatase TiO_2.[33] The absorption of the TiO_2/GO/$CuFe_2O_4$ nanocomposite extended to the visible light region, and this observation is attributed to the creation of

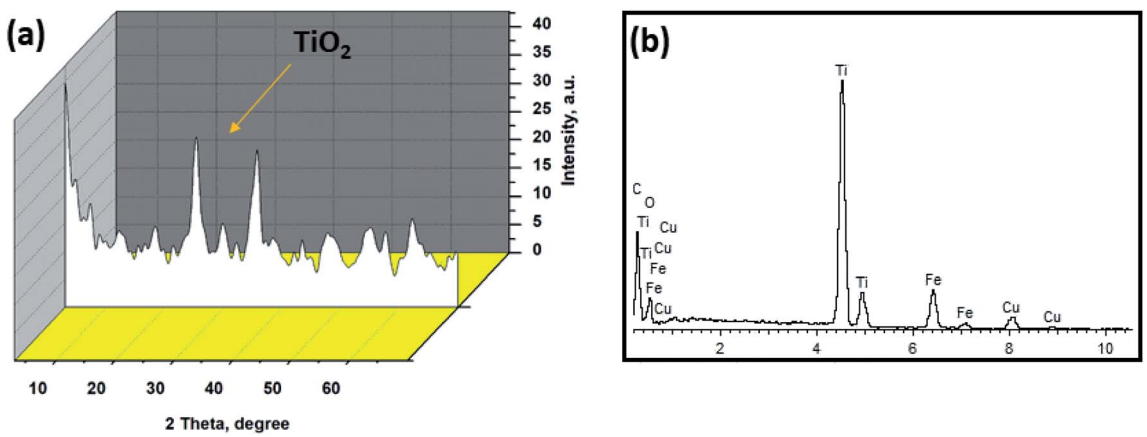

Fig. 1 (a) X-ray diffraction pattern and (b) EDX analysis of the as-synthesized TiO_2/GO/$CuFe_2O_4$ nanocomposite.

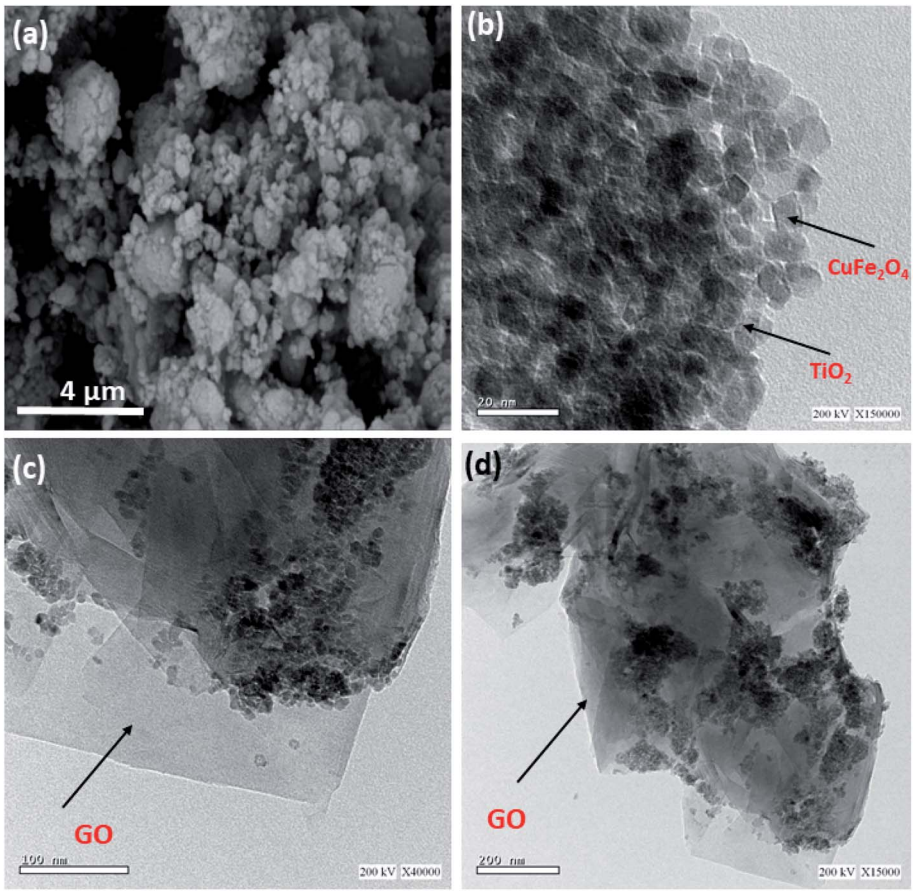

Fig. 2 (a) SEM and (b–d) TEM images of the as-synthesized TiO_2/GO/$CuFe_2O_4$ nanocomposite.

a new valence band resulting from the hybridization of C_{2p} and O_{2p} atomic orbitals.[34] In this study, the bandgap energy is calculated from the Kubelka–Munk theory and was found to be 2.4 eV (Fig. 3b), which is lower than that reported in the literature for pure TiO_2 (E_g = 3.2 eV).[9,14,16,35] The formation of the TiO_2/GO/$CuFe_2O_4$ nanocomposite causes a narrowing in the TiO_2 bandgap due to the good interactions between TiO_2 and GO in the nanocomposite structure; therefore, GO enhanced the absorption of TiO_2 in the visible light region.

3.2. Photodegradation of pesticides using TiO_2/GO/$CuFe_2O_4$ nanocomposite

At the beginning of each experiment, the collectors were stirred for about 10 min to homogenize the solution. The initial

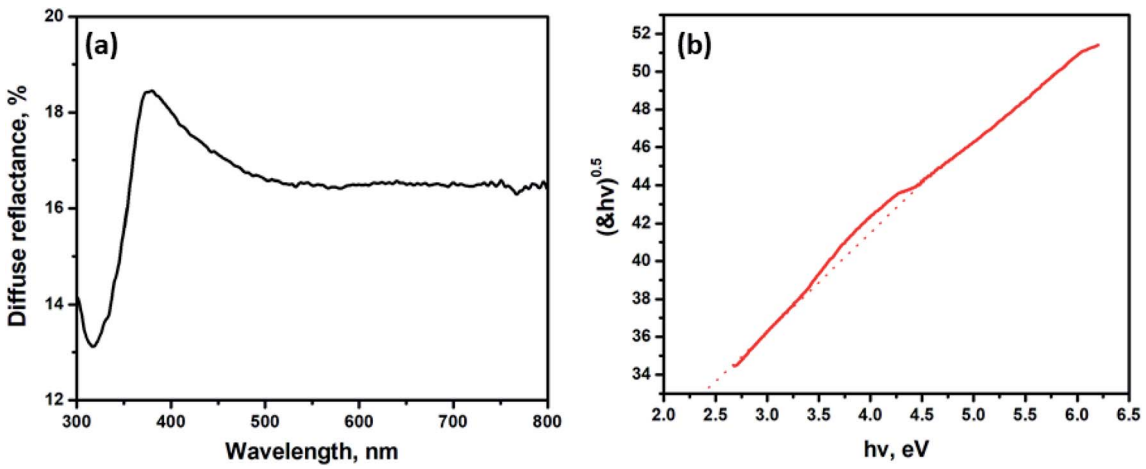

Fig. 3 (a) Diffuse reflectance spectrum and (b) Tauc plot of the TiO_2/GO/$CuFe_2O_4$ nanocomposite.

Table 1 The retention times of the different pesticides and their photocatalytic decomposition in absence and presence of UV illumination catalyzed by TiO_2/GO/$CuFe_2O_4$ nanocomposite

Pesticide	Retention time	Initial concentration (ppb)	Concentration after 20 min (dark conditions)	Concentration after 20 min UV illumination
A-BHC	8.965	924.75	357.83	71.99
B-BHC	9.871	967.82	283.90	63.31
G-BHC	10.114	953.25	411.01	121.08
D-BHC	11.021	777.78	389.23	228.17
Heptachlor	13.033	928.64	418.29	261.95
Aldrine	14.607	933.76	178.25	37.86
Heptachlor epoxide	16.586	820.17	312.27	87.87
Endosulfan (1)	18.420	768.24	309.41	103.52
Dieldrine	19.790	701.61	318.23	106.17
DDE	19.970	910.79	164.66	31.74
Endrine	20.921	679.51	392.83	73.01
Endosulfan (2)	21.463	725.27	299.78	152.21
DDD	22.170	778.29	344.69	186.04
Endrine aldehyde	22.525	746.55	311.87	220.34
Endosulfane sulfate	23.833	694.52	549.93	469.42
DDT	24.212	688.98	352.03	278.33
Methoxychlor	28.059	561.10	408.90	321.05

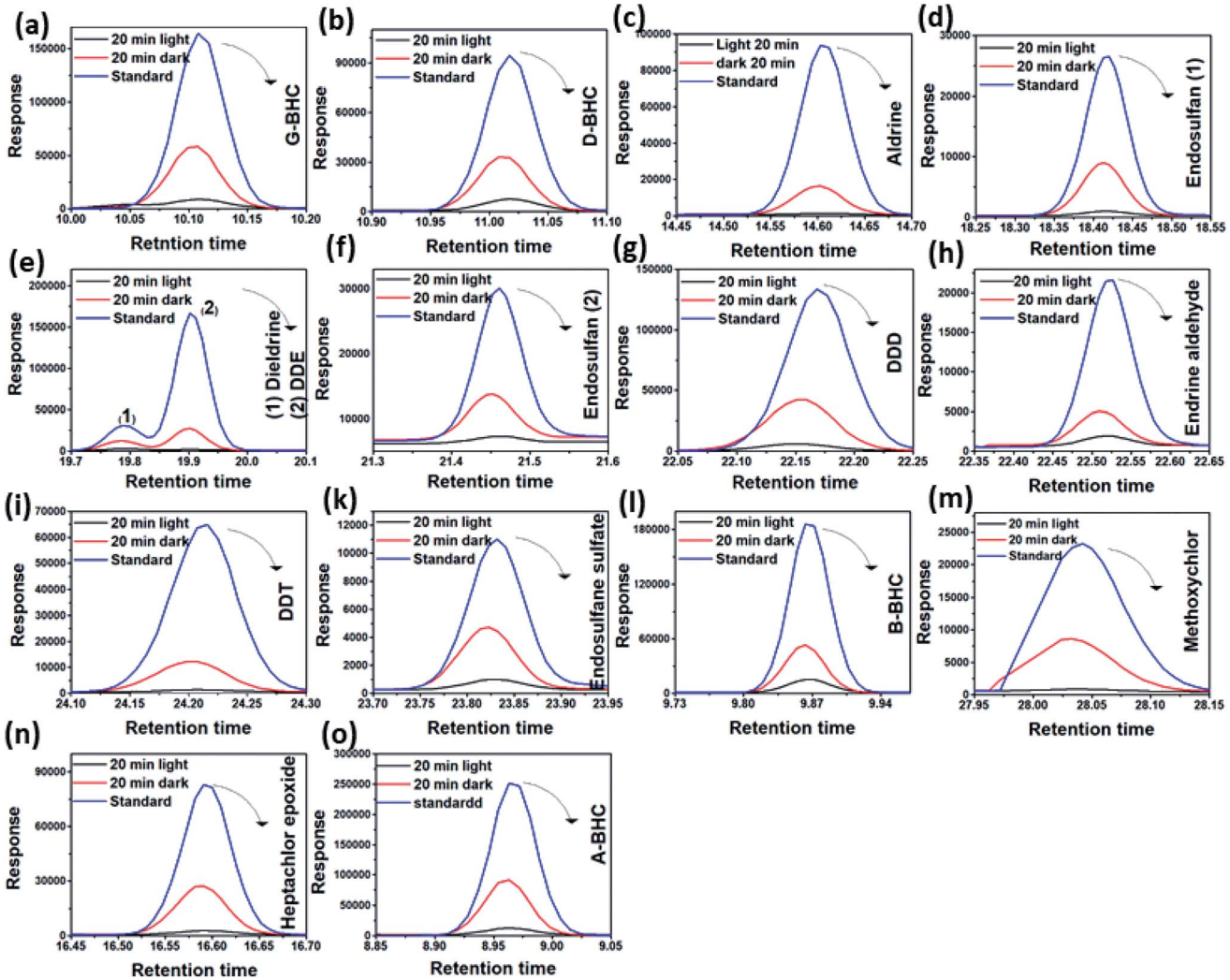

Fig. 4 (a–o) Peak elution change of selected pesticides *vs.* retention times using the TiO_2/GO/$CuFe_2O_4$ nanocomposite.

concentration of pesticides was 0.5 mg L^{-1}. During the experiments of photocatalytic degradation, GC was used to detect the produced materials. The retention times of the different pesticides and their photocatalytic decomposition in the absence and presence of UV illumination are shown in Table 1. Fig. 4 shows the results of the photocatalytic degradation of 17 pesticides in aqueous solution using the TiO_2/GO/$CuFe_2O_4$ nanocomposite. Fig. 4a–o depicts the photodegradation curves of some pesticides using the TiO_2/GO/$CuFe_2O_4$ catalyst in the absence and presence of UV illumination (365 nm). All tested pesticides were sufficiently removed without and with UV irradiation. Photocatalysis of pesticides involves two steps, *i.e.*, (i) adsorption onto the TiO_2/GO/$CuFe_2O_4$ nanocomposite surface followed by (ii) photodegradation in the presence of UV radiation.

The use of graphene enhanced significantly the degradation of pesticides in the dark. It has been reported that a C–Ti or C–O–Ti bond acts as a dopant in TiO_2 or $CuFe_2O_4$, leading to the TiO_2/GO/$CuFe_2O_4$ nanocomposite being a visible-light-driven photocatalyst. Furthermore, GO could enhance the e^-–h^+ separation through its π–π stacking between pesticides and an aromatic group of GO.[36–38] Fig. 5a shows the normalized concentration change (C/C_0) *versus* degradation time for the TiO_2/GO/$CuFe_2O_4$ nanocomposite, where C_0 is initial concentration and C is the concentration of pesticide at time *t*. At the end of the experiment, the remaining concentration of pesticides ranged from 20.8% for endosulfane sulfate to 70% for B-BHC. Under UV irradiation, the degradation of pesticide reached 96.5% for DDE.

Kinetic information indicated that the experimental data were best fitted with a pseudo-first-order linear transformation[39] as presented in Fig. 5b:

$$\ln(C/C_0) = -kt \quad (1)$$

where *k* is the rate constant of a pseudo-first-order reaction. Upon UV light illumination, DDE is completely degraded by TiO_2/GO/$CuFe_2O_4$ photocatalyst, and the degradation rate constant is 0.0838 min^{-1} (Fig. 5c).

3.3. Repeated use of the TiO_2/GO/$CuFe_2O_4$ photocatalyst

Repeated use of a photocatalyst is an essential issue in the practical application of a catalysis process. When using TiO_2 as a photocatalyst, it is difficult to effectively recover the catalyst

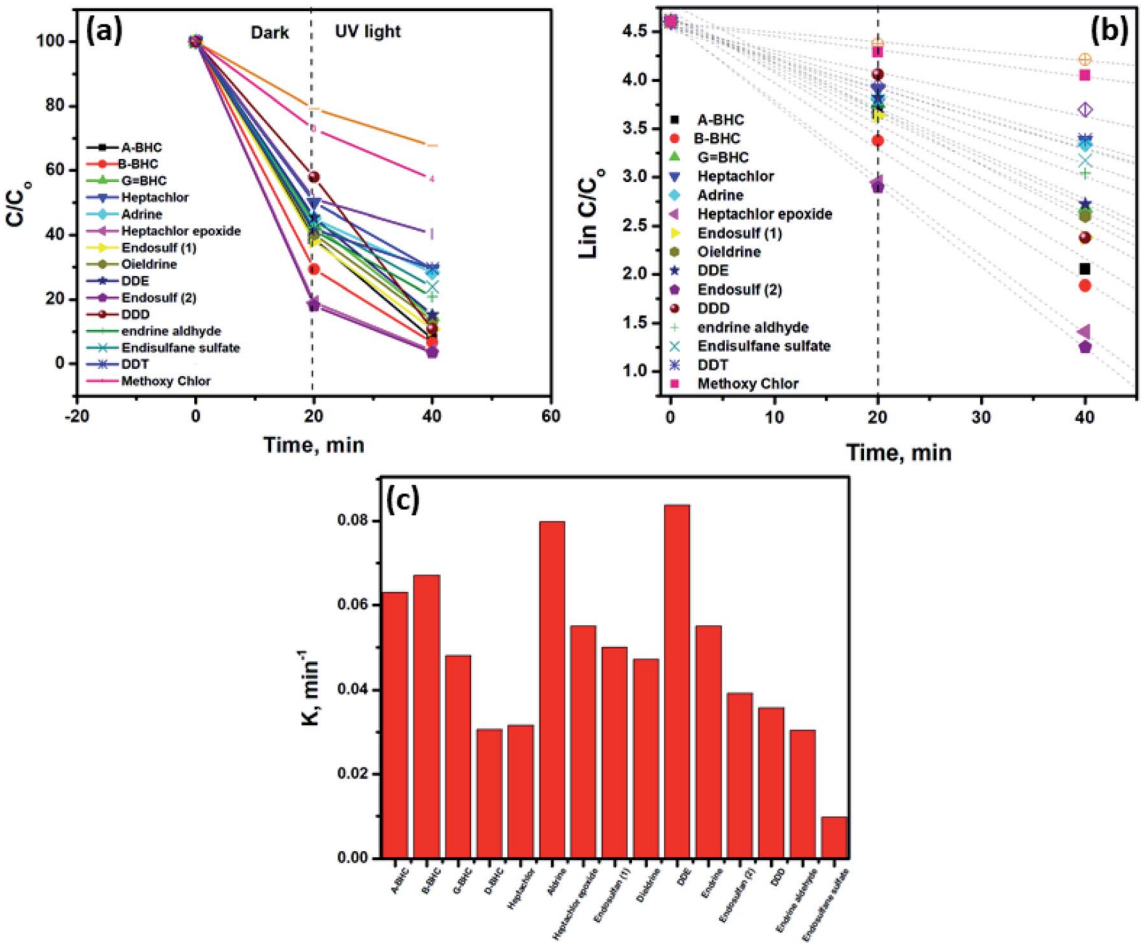

Fig. 5 (a) Removal efficiency of selected pesticides as a function of irradiation time, (b) ln(C/C_0) *vs.* time (min) curve for photodegradation of selected pesticides and (c) photodegradation rate in the presence of the TiO_2/GO/$CuFe_2O_4$ nanocomposite.

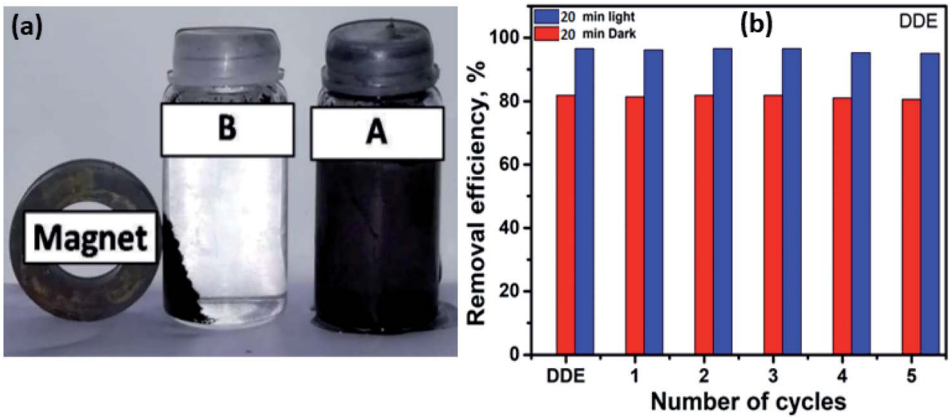

Fig. 6 (a) Photograph of the magnetic nanocomposite solution, (b) the recyclability of DDE-type pesticide by the TiO_2/GO/$CuFe_2O_4$ nanocomposite.

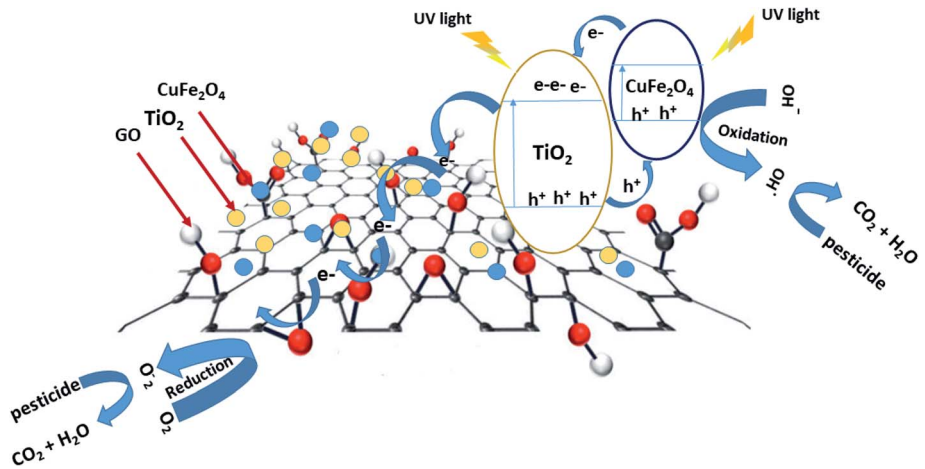

Fig. 7 Proposed mechanism of charge separation *via* a direct Z-type scheme under UV illumination.

from the photocatalytic reactor, even with the assistance of high-speed centrifugation. Consequently, loss of photocatalyst and decrease of its photocatalytic activity are noticed in subsequent recycling processes. In addition to the higher catalytic effect of the prepared nanocomposite catalyst, it can be simply isolated from the reaction medium by using a magnet (see Fig. 6a). The recovered photocatalyst was used for 5 cycles without any noticeable loss in activity and efficiency; see Fig. 6b for the photodegradation efficiency with DDE. As an example of the tested pesticides, DDE was subjected to photodegradation with recovered catalyst, and the catalytic activity almost remained the same even after 5 cycles, where the removal efficiency reached 95.05%.

3.4. Mechanism of action of TiO_2/GO/$CuFe_2O_4$

The mechanism proposed for an explanation of the enhancement of photocatalytic degradation of pesticides over the TiO_2/GO/$CuFe_2O_4$ nanocomposite is illustrated in Fig. 7. Under the irradiation of UV light, there is excitation of electrons in the valence band (VB) to the conduction band (CB) of both semiconductors TiO_2 and $CuFe_2O_4$ and leaving holes behind. The photoexcited electrons of $CuFe_2O_4$ would transfer to TiO_2, as the CB of $CuFe_2O_4$ is more negative than the CB of TiO_2, and the holes of the VB of TiO_2 would simultaneously migrate to the VB of $CuFe_2O_4$. After that, the GO sheet which is interfacially in contact with TiO_2 and $CuFe_2O_4$ nanoparticles can capture the photogenerated electrons and act as a charge carrier for the electrons.[40] The pesticide molecules can be adsorbed on the surface of the nanocomposite with conjugation among pesticide and aromatic regions of GO as proved by the high adsorption capacity of pesticides on the TiO_2/GO/$CuFe_2O_4$ nanocomposite. The remaining holes can directly oxidize the adsorbed pesticide and form hydroxyl radicals ($^{\bullet}OH$) and superoxide radicals ($O_2^{\bullet-}$) to produce CO_2 and H_2O as a non-toxic product. Therefore, the high photocatalytic activity of the TiO_2/GO/$CuFe_2O_4$ nanocomposite is related to the high charge separation and easy transfer of photoinduced charge carriers according to the GO-promoted Z-scheme mechanism.

4. Conclusion

A TiO_2/GO/$CuFe_2O_4$ nanocomposite was prepared by physical mixing of nanomaterials by a facile ball-milling approach. The

structure of the nanocomposite was characterized using XRD, EDX, SEM, and TEM techniques. Typically, TEM analysis indicated that the TiO_2 and $CuFe_2O_4$ nanoparticles, with a mean diameter of 10–15 nm, were homogeneously dispersed over the GO layers. The photocatalyst exhibits a high removal efficiency for 17 different chlorinated pesticides (persistent organic pollutants) under UV light. The catalyst is easily isolated from the reaction medium and reused for at least 5 cycles. These promising findings will shed light on the expected utilization of the TiO_2/GO/$CuFe_2O_4$ nanocomposite in various photocatalytic applications to address environmental/energy issues such as carbon dioxide reduction, hydrogen production, and solar cells.

Conflicts of interest

There are no conflicts to declare.

Acknowledgements

This work was funded by the Science & Technology Development Fund in Egypt (STDF), grant no. 19665, and Central Metallurgical Research and Development Institute (CMRDI), and they are much appreciated for their support.

References

1 J. K. Summers, L. M. Smith, J. L. Case and R. A. Linthurst, A review of the elements of human well-being with an emphasis on the contribution of ecosystem services, *Ambio*, 2012, **41**(4), 327–340, DOI: 10.1007/s13280-012-0256-7.

2 E. C. Lima, Removal of emerging contaminants from the environment by adsorption, *Ecotoxicol. Environ. Saf.*, 2018, **150**, 1–17, DOI: 10.1016/j.ecoenv.2017.12.026.

3 M. N. Rashed, Adsorption technique for the removal of organic pollutants from water and wastewater, in *Organic pollutants-monitoring, risk and treatment*, IntechOpen, 2013, DOI: 10.5772/54048.

4 I. Ali, New generation adsorbents for water treatment, *Chem. Rev.*, 2012, **112**(10), 5073–5091, DOI: 10.1021/cr300133d.

5 Y. Huang, L. Xiao, F. Li, M. Xiao, D. Lin, X. Long and Z. Wu, Microbial degradation of pesticide residues and an emphasis on the degradation of cypermethrin and 3-phenoxy benzoic acid: a review, *Molecules*, 2018, **23**(9), 2313, DOI: 10.3390/molecules23092313.

6 J. Jacob, A Review of the accumulation and distribution of persistent organic pollutants in the environment, *Int. J. Biosci., Biochem. Bioinf.*, 2013, **3**(6), 657, DOI: 10.7763/IJBBB.2013.V3.297.

7 M. A. Quiroz, E. R. Bandala and C. A. Martínez-Huitle, Advanced oxidation processes (AOPs) for removal of pesticides from aqueous media, in *Pesticides-Formulations, effects, fate*, IntechOpen, 2011, DOI: 10.5772/1004.

8 C. Amor, L. L. Marchão, M. S. Lucas and J. A. Peres, Application of advanced oxidation processes for the treatment of recalcitrant agro-industrial wastewater: a review, *Water*, 2019, **11**(2), 205, DOI: 10.3390/w11020205.

9 M. A. Hamza, Z. M. Abou-Gamra and M. A. Ahmed, The critical role of Tween 80 as a 'green' template on the physical properties and photocatalytic performance of TiO_2 nanoparticles for Rhodamine B photodegradation, *J. Mater. Sci.: Mater. Electron.*, 2020, **31**, 4650–4661, DOI: 10.1007/s10854-020-03017-2.

10 A. N. El-Shazly, M. M. Rashad, E. A. Abdel-Aal, I. A. Ibrahim, M. F. El-Shahat and A. E. Shalan, Nanostructured ZnO photocatalysts prepared *via* surfactant assisted Co-Precipitation method achieving enhanced photocatalytic activity for the degradation of methylene blue dyes, *J. Environ. Chem. Eng.*, 2016, **4**, 3177–3184, DOI: 10.1016/j.jece.2016.06.018.

11 M. A. Hamza, A. N. El-Shazly, S. A. Tolba and N. K. Allam, Novel Bi-based photocatalysts with unprecedented visible light driven hydrogen production rate: experimental and DFT insights, *Chem. Eng. J.*, 2020, **348**, 123351, DOI: 10.1016/j.cej.2019.123351.

12 M. A. Hamza, A. N. El-Shazly and N. K. Allam, Facile template-free one-pot room-temperature synthesis of novel m-$Bi(OH)CrO_4$ microspheres, *Mater. Lett.*, 2020, **262**, 127188, DOI: 10.1016/j.matlet.2019.127188.

13 S. Nabih, A. E. Shalan, E. S. A. Serea, M. A. Goda and M. F. Sanad, Photocatalytic performance of TiO_2@ SiO_2 nanocomposites for the treatment of different organic dyes, *J. Mater. Sci.: Mater. Electron.*, 2019, **30**(10), 9623–9633, DOI: 10.1007/s10854-019-01296-y.

14 M. A. Ahmed, Z. M. Abou-Gamra, H. A. A. Medien and M. A. Hamza, Effect of porphyrin on photocatalytic activity of TiO_2 nanoparticles toward Rhodamine B photodegradation, *J. Photochem. Photobiol., B*, 2017, **176**, 25–35, DOI: 10.1016/j.jphotobiol.2017.09.016.

15 A. El-Sayed, N. Atef, A. H. Hegazy, K. R. Mahmoud, R. A. Hameed and N. K. Allam, Defect states determined the performance of dopant-free anatase nanocrystals in solar fuel cells, *Sol. Energy*, 2017, **144**, 445–452, DOI: 10.1016/j.solener.2017.01.056.

16 Z. M. Abou-Gamra, M. A. Ahmed and M. A. Hamza, Investigation of commercial $PbCrO_4$/TiO_2 for photodegradation of rhodamine B in aqueous solution by visible light, *Nanotechnol. Environ. Eng.*, 2017, **2**, 12, DOI: 10.1007/s41204-017-0024-9.

17 A. N. El-Shazly, A. H. Hegazy, M. M. Rashad, M. F. El-Shahat and N. K. Allam, Ultrathin ALD TiO_2 shells for enhanced photoelectrochemical solar fuel generation, *J. Alloys Compd.*, 2018, **739**, 178–183, DOI: 10.1016/j.jallcom.2017.12.218.

18 M. Y. Rezk, M. Zeitoun, A. N. El-Shazly, M. M. Omar and N. K. Allam, Robust photoactive nanoadsorbents with antibacterial activity for the removal of dyes, *J. Hazard. Mater.*, 2019, **378**, 120679, DOI: 10.1016/j.jhazmat.2019.05.072.

19 H. Cheng, J. Wang, Y. Zhao and X. Han, Effect of phase composition, morphology, and specific surface area on the photocatalytic activity of TiO_2 nanomaterials, *RSC Adv.*, 2014, **4**(87), 47031–47038, DOI: 10.1039/C4RA05509H.

20 Á. Tolosana-Moranchel, A. Manassero, M. L. Satuf, O. M. Alfano, J. A. Casas and A. Bahamonde, Influence of TIO_2-rGO optical properties on the photocatalytic activity and efficiency to photodegrade an emerging pollutant, *Appl. Catal., B*, 2019, **246**, 1–11, DOI: 10.1016/j.apcatb.2019.01.054.

21 D. L. Cunha, A. Kuznetsov, J. R. Araujo, R. S. Neves, B. S. Archanjo, M. C. Canela and M. Marques, Optimization of Benzodiazepine Drugs Removal from Water by Heterogeneous Photocatalysis Using TiO_2/Activated Carbon Composite, *Water, Air, Soil Pollut.*, 2019, **230**(7), 141, DOI: 10.1007/s11270-019-4202-1.

22 N. Ahmed, M. Ramadan, W. M. El Rouby, A. A. Farghali and N. K. Allam, Non-precious co-catalysts boost the performance of TiO2 hierarchical hollow mesoporous spheres in solar fuel cells, *Int. J. Hydrogen Energy*, 2018, **43**(46), 21219–21230.

23 L. K. Putri, L. L. Tan, W. J. Ong, W. S. Chang and S. P. Chai, Graphene oxide: exploiting its unique properties toward visible-light-driven photocatalysis, *Appl. Mater. Today*, 2016, **4**, 9–16, DOI: 10.1016/j.apmt.2016.04.001.

24 N. R. Khalid, E. Ahmed, Z. Hong, L. Sana and M. Ahmed, Enhanced photocatalytic activity of graphene–TiO_2 composite under visible light irradiation, *Curr. Appl. Phys.*, 2013, **13**(4), 659–663, DOI: 10.1016/j.cap.2012.11.003.

25 X. Rong, F. Qiu, C. Zhang, L. Fu, Y. Wang and D. Yang, Preparation, characterization and photocatalytic application of TiO2–graphene photocatalyst under visible light irradiation, *Ceram. Int.*, 2015, **41**(2), 2502–2511, DOI: 10.1016/j.ceramint.2014.10.072.

26 Y. Lin, Z. Geng, H. Cai, L. Ma, J. Chen, J. Zeng and X. Wang, Ternary graphene–TiO_2–Fe_3O_4 nanocomposite as a recollectable photocatalyst with enhanced durability, *Eur. J. Inorg. Chem.*, 2012, **28**, 4439–4444, DOI: 10.1002/ejic.201200454.

27 H. Yao, M. Fan, Y. Wang, G. Luo and W. Fei, Magnetic titanium dioxide based nanomaterials: synthesis, characteristics, and photocatalytic application in pollutant degradation, *J. Mater. Chem. A*, 2015, **3**(34), 17511–17524, DOI: 10.1039/C5TA03215F.

28 M. Gebrezgiabher, G. Gebreslassie, T. Gebretsadik, G. Yeabyo, F. Elemo, Y. Bayeh and W. Linert, A C-Doped TiO_2/Fe_3O_4 Nanocomposite for Photocatalytic Dye Degradation under Natural Sunlight Irradiation, *J. Compos. Sci.*, 2019, **3**(3), 75, DOI: 10.3390/jcs3030075.

29 H. Mozafari and S. Azarakhsh, Photodegradation of azo dyes: photocatalyst and magnetic investigation of $CoFe_2O_4$–TiO_2–Ag nanocomposites, *J. Mater. Sci.: Mater. Electron.*, 2018, **29**(7), 5993–6003.

30 M. O. Ojemaye, O. O. Okoh and A. I. Okoh, Performance of $NiFe_2O_4$-SiO_2-TiO_2 magnetic photocatalyst for the effective photocatalytic reduction of Cr (VI) in aqueous solutions, *J. Nanomater.*, 2017, **2017**, 1–11, DOI: 10.1155/2017/5264910.

31 Q. Xu, J. Feng, L. Li, Q. Xiao and J. Wang, Hollow $ZnFe_2O_4$/TiO_2 composites: high-performance and recyclable visible-light photocatalyst, *J. Alloys Compd.*, 2015, **641**, 110–118, DOI: 10.1016/j.jallcom.2015.04.076.

32 T. B. Nguyen and R. A. Doong, Fabrication of highly visible-light-responsive $ZnFe_2O_4$/TiO_2 heterostructures for the enhanced photocatalytic degradation of organic dyes, *RSC Adv.*, 2016, **6**(105), 103428–103437.

33 R. Plass, S. Pelet, J. Krueger, M. Grätzel and U. Bach, Quantum dot sensitization of organic– inorganic hybrid solar cells, *J. Phys. Chem. B*, 2002, **106**(31), 7578–7580, DOI: 10.1021/jp020453l.

34 R. Sedghi and F. Heidari, A novel & effective visible light-driven TiO_2/magnetic porous graphene oxide nanocomposite for the degradation of dye pollutants, *RSC Adv.*, 2016, **6**(55), 49459–49468, DOI: 10.1039/C6RA02827F.

35 R. Nosrati, A. Olad and S. Shakoori, Preparation of an antibacterial, hydrophilic and photocatalytically active polyacrylic coating using TiO_2 nanoparticles sensitized by graphene oxide, *Mater. Sci. Eng., C*, 2017, **80**, 642–651, DOI: 10.1016/j.msec.2017.07.004.

36 C. Chen, W. Cai and M. Long, Synthesis of visible-light responsive graphene oxide/TiO_2 composites with p/n heterojunction, *ACS Nano*, 2010, **4**, 6425–6432, DOI: 10.1021/nn102130m.

37 Y. Zhang, Z. R. Tang, X. Fu, *et al.*, Engineering the unique 2D mat of graphene to achieve graphene–TiO2 nanocomposite for photocatalytic selective transformation: what advantage does graphene have over its forebear carbon nanotube?, *ACS Nano*, 2011, **5**, 7426–7435, DOI: 10.1021/nn202519j.

38 Y. Zhang, N. Zhang and Z. R. Tang, Improving the photocatalytic performance of graphene–TiO_2 nanocomposites *via* a combined strategy of decreasing defects of graphene and increasing interfacial contact, *Phys. Chem. Chem. Phys.*, 2012, **14**, 9167–9175.

39 D. Bamba, P. Atheba, D. Robert, A. Trokourey and B. Dongui, Photocatalytic degradation of the diuron pesticide, *Environ. Chem. Lett.*, 2008, **6**(3), 163–167, DOI: 10.1007/s10311-007-0118-x.

40 A. N. El-Shazly, M. Y. Rezk, K. M. Gameel and N. K. Allam, Electrospun Lead-Free All-Inorganic Double Perovskite Nanofibers for Photovoltaic and Optoelectronic Applications, *ACS Appl. Nano Mater.*, 2019, **2**(11), 7085–7094, DOI: 10.1021/acsanm.9b01613.

